


## RESEARCH ARTICLE OPEN ACCESS

# Identification of a Biomarker Panel in Extracellular Vesicles Derived From Non-Small Cell Lung Cancer (NSCLC) Through Proteomic Analysis and Machine Learning

Ye Yuan<sup>1,2</sup> | Hai Jiang<sup>4</sup> | Rui Xue<sup>4</sup> | Xiao-Jun Feng<sup>1</sup> | Bi-Feng Liu<sup>1</sup> | Lian Li<sup>4</sup> | Bo Peng<sup>2</sup> | Chen-Shuo Ren<sup>2</sup> | Shi-Min Li<sup>2</sup> | Na Li<sup>2</sup> | Min Li<sup>2</sup> | Dian-Bing Wang<sup>2</sup> | Xian-En Zhang<sup>2,3</sup> 

<sup>1</sup>College of Life Science and Technology, Huazhong University of Science and Technology, Wuhan, P. R. China | <sup>2</sup>Key Laboratory of Biomacromolecules (CAS), Institute of Biophysics, Chinese Academy of Sciences, Beijing, China | <sup>3</sup>Faculty of Synthetic Biology, Shenzhen University of Advanced Technology, Shenzhen, China | <sup>4</sup>Renmin Hospital, Hubei University of Medicine, Shiyan, P. R. China

**Correspondence:** Dian-Bing Wang ([wangdb@moon.ibp.ac.cn](mailto:wangdb@moon.ibp.ac.cn)) | Xian-En Zhang ([zhangxe@ibp.ac.cn](mailto:zhangxe@ibp.ac.cn))

**Received:** 20 September 2024 | **Revised:** 20 March 2025 | **Accepted:** 31 March 2025

**Funding:** This study was supported by the National Natural Science Foundation of China (21890743 and 32271489), the National Key Research and Development Program of China (2022YFA1205804 and 2022YFC2303501).

**Keywords:** biomarkers | diagnosis | extracellular vesicles | NSCLC | proteomics

## ABSTRACT

Antigen fingerprint profiling of tumour-derived extracellular vesicles (TDEVs) in the body fluids is a promising strategy for identifying tumour biomarkers. In this study, proteomic and immunological assays reveal significantly higher CD155 levels in plasma extracellular vesicles (EVs) from patients with non-small cell lung cancer (NSCLC) than from healthy individuals. Utilizing CD155 as a bait protein on the EV membrane, CD155+ TDEVs are enriched from NSCLC patient plasma EVs. In the discovery cohort, 281 differentially expressed proteins are identified in TDEVs of the NSCLC group compared with the healthy control group. In the verification cohort, 49 candidate biomarkers are detected using targeted proteomic analysis. Of these, a biomarker panel of seven frequently and stably detected proteins—MVP, GYS1, SERPINA3, HECTD3, SERPING1, TPM4, and APOD—demonstrates good diagnostic performance, achieving an area under the curve (AUC) of 1.0 with 100% sensitivity and specificity in receiver operating characteristic (ROC) curve analysis, and 92.3% sensitivity and 88.9% specificity in confusion matrix analysis. Western blotting results confirm upregulation trends for MVP, GYS1, SERPINA3, HECTD3, SERPING1 and APOD, and TPM4 is downregulated in EVs of NSCLC patients compared with healthy individuals. These findings highlight the potential of this biomarker panel for the clinical diagnosis of NSCLC.

## 1 | Introduction

Lung cancer, the leading cause of cancer-related deaths worldwide, is a significant public health concern (Williams et al. 2023). Non-small cell lung cancer (NSCLC), primarily lung adenocarcinoma (LUAD) and lung squamous cell carcinoma (LUSC),

constitutes 80%–90% of all lung cancer cases (Molina et al. 2008). Although lung cancer mortality rates have declined with the recent advancements in clinical diagnostics, such as imaging, pathology, molecular typing and liquid biopsy, >70% of patients with lung cancer are still diagnosed at an advanced stage (Herbst et al. 2018; Siegel et al. 2024; Sun et al. 2024). Moreover, the

Ye Yuan, Hai Jiang and Rui Xue contributed equally to this work.

This is an open access article under the terms of the [Creative Commons Attribution-NonCommercial-NoDeriv](https://creativecommons.org/licenses/by-nc-nd/4.0/) License, which permits use and distribution in any medium, provided the original work is properly cited, the use is non-commercial and no modifications or adaptations are made.

© 2025 The Author(s). *Journal of Extracellular Vesicles* published by Wiley Periodicals LLC on behalf of International Society for Extracellular Vesicles.

5-year survival rate of patients with lung cancer remains poor, and patients with advanced-stage lung cancer have poorer treatment outcomes than those diagnosed at an early stage (Tan et al. 2022; Wang et al. 2022; Reck and Rabe 2017). Therefore, early diagnosis and intervention are essential for significantly improving patient survival.

Biomarkers are used to evaluate normal and pathological biological processes or responses to exposure or intervention, including therapies (Group F-NBW 2016). Tumour liquid biopsy includes the assessment of a series of biomarkers, including serum tumour markers, circulating tumour cells (CTCs), circulating tumour DNA (ctDNA), circulating autoantibodies, and tumour-derived extracellular vesicles (TDEVs) (Fitzgerald et al. 2022; Hu et al. 2021). These non-invasive or minimally invasive biomarkers enable early cancer diagnosis and continuous monitoring of tumour dynamics, including early therapeutic resistance, residual disease and recurrence.

The molecular profiles of extracellular vesicles (EVs) are similar to those of their parent cells (Jeppesen et al. 2019). EVs are submicron- or micron-sized vesicles secreted by cells, surrounded by a lipid bilayer, and incapable of self-replication (Dixon et al. 2023). Compared with other circulating biomarkers, EVs have distinct advantages owing to their abundance, stability, and diverse expression profiles. However, it has several limitations as it is an emerging technology. Compared with tissue biopsies, standardized operating procedures for liquid biopsies encompassing the complex and diverse preparation processes for EVs remain lacking, and interference from normal cell-derived EVs complicates the definitive attribution of EV biomarkers to tumour cells (Lane et al. 2018). Moreover, the tumour markers carried by EVs are not yet fully characterized. Therefore, TDEVs primarily serve as adjunctive diagnostic tools.

TDEVs carry antigens from tumour cells, which remodel the tumour microenvironment and influence systemic antitumor responses early in the disease. The molecular profiles of TDEVs evolve with tumour progression or treatment response, exhibiting spatiotemporal specificity (Poggio et al. 2019; Qi et al. 2022; Xu et al. 2018). Therefore, cancer-related biomarkers can be effectively identified using TDEVs (Lei et al. 2023; Thuya et al. 2023). However, research and clinical application of TDEVs are challenging as they constitute only a small portion of the highly heterogeneous circulating EVs (Barlin et al. 2023).

Extensive research has focused on the molecular profiles of total EVs from various tumour types, including EVs derived from lung cancer cell lines and the plasma of patients with lung cancer (Hoshino et al. 2020; Jakobsen et al. 2015). However, few studies have isolated and characterized TDEVs from the total EVs in the plasma of patients with NSCLC. Notably, miRNA profiling of TDEVs immunocaptured with anti-EpCAM antibody, miRNAs specific to LUAD and LUSC, and a miRNA biomarker panel for the diagnosis of NSCLC have been identified (Jin et al. 2017). However, a comprehensive proteomic analysis of TDEVs in the circulation of patients with NSCLC has not yet been reported. Therefore, a detailed understanding of the tumour antigen fingerprints of NSCLC TDEVs remains lacking.

This study aimed to establish a molecular profile of NSCLC TDEVs distinct from that of healthy individuals through comparative proteomics. Notably, CD155, as a transmembrane glycoprotein, is strongly relevant to NSCLC deterioration and was found to be significantly elevated in NSCLC tumour tissues and plasma EVs. Subsequently, CD155 served as a bait for the immunocapture of CD155+ TDEVs from the plasma EVs of patients with NSCLC. We then analysed differentially expressed proteins (DEPs) in these TDEVs and compared them with those in the plasma EVs of healthy individuals. Furthermore, these DEPs were quantitatively detected through targeted proteomics to identify a panel of seven proteins (MVP, GYS1, SERPINA3, HECTD3, SERPING1, TPM4 and APOD) with excellent diagnostic potential for NSCLC using stepwise machine learning.

## 2 | Materials and Methods

### 2.1 | Cell Lines and Cell Culture

Human NSCLC cell lines (A549, H1975, H460 and SK-MES-1) were obtained from the National Infrastructure of Cell Line Resource. Human bronchial epithelial cell lines (BEAS-2B and BEP-2D), a human alveolar epithelial cell line (HPAEPiC) and HEK293T were obtained from BioDee (Beijing, China). SK-MES-1 cells were cultured in MEM basic medium (Gibco, C11095500BT) supplemented with 10% foetal bovine serum (FBS) (GenStar, #C504-10), and penicillin–streptomycin (Macgene, CC004). The remaining cells were cultured in DMEM medium (Gibco, C11995500BT) supplemented with 10% FBS and penicillin–streptomycin. For the isolation of EVs, when the cells reached approximately 80% confluence, they were cultured in medium without FBS. All cell lines were maintained in a humidified incubator at 37°C with 5% CO<sub>2</sub> and screened regularly to ensure that they were free of *Mycoplasma* contamination.

### 2.2 | Clinical Specimens

A total of 355 plasma samples were collected from 108 patients with LUAD, 31 patients with LUSC, and 216 healthy individuals at Shiyuan Renmin Hospital. All the donors provided informed consent to participate in this study. Detailed clinical information regarding healthy controls and patients with NSCLC is presented in Table S1. This study was conducted in accordance with the International Ethical Guidelines for Biomedical Research Involving Human Subjects and approved by the Research Ethics Committee of Renmin Hospital, Hubei University of Medicine. Blood samples were collected from donors in the morning after an overnight fast. Using a 22-gauge straight needle, blood was drawn from the median cubital vein with mild tourniquet application. A total of 3 mL of peripheral blood was collected from each donor. The blood collection tubes were gently inverted 6–10 times to ensure thorough mixing of the anticoagulant with the blood. The tubes were then transported in a medical insulated box (4–8°C) to the laboratory within 15 min. The blood was centrifuged at 1500 × g for 10 min at 4°C, and the resulting plasma was transferred to a new tube and centrifuged again at 2500 × g for 10 min at 4°C. After centrifugation, the plasma was aliquoted into a clean polypropylene centrifuge tube and stored at –80°C until EV isolation. Tissue microarrays (TMAs) included

75 NSCLC tumour tissue samples (30 LUSC, 35 LUAD, seven adenosquamous carcinomas and three large cell carcinomas), and 75 paired adjacent lung tissue samples were purchased from Shanghai Outdo Biotech. The preparation of TMAs was approved by the Research Ethics Committee of Shanghai Outdo Biotech.

We randomly selected 19 plasma samples from a control group of 133 healthy individuals and pooled them at 13 mL per sample for the quantitative proteomics of immunocaptured EVs. Similarly, we selected nine plasma samples from 45 individuals diagnosed with NSCLC and pooled them at the same volume. Individual plasma samples were used for parallel reaction monitoring (PRM) verification and immunological detection.

### 2.3 | Isolation of EVs

EVs were isolated from plasma or culture supernatants via sequential ultracentrifugation. The plasma EV isolation process followed the Standardized Reporting Tool for Blood EV Research (Human) (Lucien et al. 2023). Before EV isolation, quality control measurements of plasma samples were performed using a haematology analyser (HEMAVET HV950). Only plasma samples meeting the quality control criteria were used for subsequent EV isolation. Briefly, supernatants (plasma diluted 1:10 in PBS) were centrifuged at  $300 \times g$  for 10 min,  $1000 \times g$  for 15 min and  $3000 \times g$  for 20 min at  $4^{\circ}\text{C}$  to remove dead cells and debris, followed by centrifugation at  $10,000 \times g$  for 30 min at  $4^{\circ}\text{C}$  to eliminate large vesicles. After filtration through a  $0.22 \mu\text{m}$  filter, the supernatants were transferred to centrifuge bottles (Beckman Coulter, 355622) and centrifuged at  $100,000 \times g$  for 90 min at  $4^{\circ}\text{C}$  using an Optima XPN-100 ultracentrifuge. For cell culture supernatants, the pellets were resuspended in PBS and subjected to ultracentrifugation. The EV pellets were then resuspended in PBS.

For isolating total EVs from plasma, high-abundance proteins, such as immunoglobulins and albumin, were removed using protein A/G magnetic beads (MedChemExpress, HY-K0202) and immunoprecipitated with anti-albumin antibody (Sino Biological, 68001-R101). Subsequently, the samples were ultracentrifuged and resuspended in PBS.

For immunocaptured EVs, after biotinylation of anti-CD155 (Sino Biological, 10109-RP02) and anti-CD63 (Santa Cruz Biotechnology, SC-5275) using a biotinylation kit (Bomeida Life Science, G-MM-IGT) following the manufacturer's protocol, 500  $\mu\text{g}$  of EVs in 500  $\mu\text{L}$  PBS were subjected to immunocapture using streptavidin magnetic beads charged with biotin-labelled antibodies. Briefly, total EVs from the NSCLC group or the healthy control group were incubated overnight at  $4^{\circ}\text{C}$  with biotin-labelled anti-CD155 or anti-CD63 antibodies, respectively. Next, 30  $\mu\text{L}$  of streptavidin magnetic beads (MedChemExpress, HY-K0208) were added to the EV-antibody complexes and incubated for 6 h at  $4^{\circ}\text{C}$ . Subsequently, the recovered bead-bound complexes were washed thrice with wash buffer (0.01% Tween 20 in PBS) and then boiled with 30  $\mu\text{L}$  of  $1\times$  SDS-PAGE loading buffer.

### 2.4 | Preparation of EV-Depleted Plasma

The diluted plasma was sequentially centrifuged at  $300 \times g$  for 10 min,  $1000 \times g$  for 15 min,  $3000 \times g$  for 20 min and

$20,000 \times g$  for 40 min at  $4^{\circ}\text{C}$ . Subsequently, the supernatant was ultracentrifuged at  $100,000 \times g$  for 16 h at  $4^{\circ}\text{C}$ . The final supernatant (EV-depleted plasma) was aliquoted and stored at  $-80^{\circ}\text{C}$  for further analysis.

### 2.5 | Construction of Stable Cell Lines

To generate a stable cell line overexpressing human CD155, the cDNA encoding CD155 was cloned into the pLVX-T2A-mCherry-Puro vector. For CD155 gene knockout (KO), a single-guide RNA (sgRNA) targeting CD155 (human CD155 sgRNA: 5'-CACCGCTGTTTCGTCACGTTCCCGCA-3', 5'-AAACTGCGGGAACGTGACGAACAGC-3') synthesized by Sangon Biotech (Beijing, China) and cloned into the lentiCRISPRv2 vector (Addgene, #52961). All constructs were verified by gene sequencing.

Lentiviruses were produced by co-transfecting HEK293T cells with third-generation packaging plasmids pMD2.G (Addgene, #12259) and psPAX2 (Addgene, #12260), and either pLVX-CD155-T2A-mCherry-Puro (for CD155 overexpression) or lentiCRISPRv2-CD155-KO (for CD155 knockout), using Lipofectamine 3000 (Thermo Fisher Scientific, L3000015). The lentiviral supernatant was collected 48 h post-transfection, filtered through a  $0.45 \mu\text{m}$  membrane, and used to transduce H1975 cells with polybrene (10  $\mu\text{g}/\text{mL}$ , Beyotime, C0351) for 48 h. Subsequently, transduced cells were then selected with puromycin (4  $\mu\text{g}/\text{mL}$ , Beyotime, ST551) for 1 week. The surviving cells were sorted using FACSaria IIIu (BD Biosciences), expanded and validated by immunoblotting and sequencing.

### 2.6 | Cell Proliferation Assay

H1975 stable cell lines (CD155-overexpressing and CD155-knockout) and wild-type H1975 cells were seeded into 96-well plates at a density of  $2 \times 10^3$  cells per well. Cell proliferation was assessed using the CCK-8 assay (LABEAD, CK001) according to the manufacturer's instructions. Briefly, 10  $\mu\text{L}$  of CCK-8 reagent was added to each well, and the plates were incubated at  $37^{\circ}\text{C}$  for 2 h. The optical density (OD) at 450 nm was measured daily for three consecutive days using a microplate reader (BIO-TEK, CYT3MFV). All experiments were performed in triplicate.

### 2.7 | Immunohistochemistry (IHC) and Immunofluorescence Staining

Immunohistochemical staining of the TMAs was performed as previously described (Jin et al. 2024). Briefly, a 1:100 dilution of an anti-CD155 antibody (Abcam, ab267788) was used, and 43 paired samples were excluded from subsequent analyses owing to partial slice escape after staining. Finally, 32 paired specimens, including 15 LUAD and 17 LUSC, were included in the subsequent analyses.

H1975 cells were cultured in confocal dishes (Nest, 801001). Cells were fixed with 4% paraformaldehyde in PBS for 10 min at room temperature ( $25^{\circ}\text{C}$ ). Subsequently, the cells were permeabilized with PBS containing 0.2% Triton X-100 (Beyotime, ST1723) for 10 min at room temperature, and then blocked with 5% goat serum (Beyotime, C0265) in PBS for 30 min at room temperature. The

samples were incubated overnight at 4°C with a 1:100 dilution of different primary antibodies, including anti-CD155 (Proteintech, 84138-1-RR), anti-CD63 (Santa Cruz Biotechnology, sc-5275), anti-Rab5 (Santa Cruz Biotechnology, sc-46692) and anti-Rab7 (Santa Cruz Biotechnology, sc-376362). After washing, the samples were incubated at 37°C for 60 min with secondary antibodies (goat anti-rabbit IgG H&L, Abcam, ab150080 or goat anti-mouse IgG H&L, Abcam, ab150113) at a 1:2000 dilution. Prior to imaging, the samples were mounted with antifade mounting medium containing DAPI (Beyotime, P0131). Images were acquired using a confocal microscope (A1R+, NIKON, Japan) equipped with 405, 488 and 594 nm lasers. Image processing, including the determination of co-localization scores of CD155 with CD63, Rab5 and Rab7, was performed using NIS-Elements AR 4.60 software (Nikon, Japan).

## 2.8 | Quantitative Analysis of IHC Staining

The TMA slides were scanned using an Aperio Scanscope CS2 (Leica Microsystems, Germany) at 200× magnification with a resolution of 0.5 µm/pixel. The background illumination levels were standardized using a pre-scan procedure. Digital images representing whole tissue sections were assessed for quality (Krajewska et al. 2009). The percentage of positive cells and the average positive intensity were quantified using the ImageScope analysis software (Aperio Technologies, USA). Scores were allocated as follows: positive area (0, <5%; 1, 5%–25%; 2, 26%–50%; 3, 51%–75%; 4, >75%) and staining intensity (0, negative; 1, weak; 2, medium; 3, strong). The final staining score was computed by multiplying the scores for staining intensity and the positive area.

## 2.9 | Characterization of EVs

To characterize the morphology of the isolated EVs, they were fixed with 2% paraformaldehyde for 5 min. Subsequently, 10 µL of the EV solution was loaded onto 300-mesh copper electron microscopy grids coated with thin formvar/carbon film, which were glow-discharged using PELCO easiGlow (PELCO, 91000). After negative staining, the EVs were examined using a Tecnai Spirit transmission electron microscopy (TEM) (FEI Company, USA) operating at 120 kV.

For immuno-electron microscopy (iEM) analysis of EVs isolated from cell lines, the grids were washed thrice with PBS after EV loading. They were then treated with 0.05M glycine for 10 min and subsequently blocked with PBS containing 1% BSA for 60 min. The grids were incubated overnight at 4°C with either an anti-CD155 antibody (Proteintech, 84138-1-RR) or rabbit IgG (Sangon Biotech, D110502), followed by incubation with anti-rabbit IgG conjugated to 10 nm gold particles (Solarbio, K1034G-G10). Finally, the grids were negatively stained and examined by TEM as described above.

To evaluate CD155 on both the surface and the lumen of plasma-derived EVs, the EVs were fixed in a mixture of 4% paraformaldehyde and 0.5% glutaraldehyde in PBS, embedded in gelatin, and infused with 2.3M sucrose. The gelatin blocks were frozen in liquid nitrogen, and ultrathin sections (80 nm) were prepared using a Leica EM FC7 ultramicrotome. The sections were

mounted on 100-mesh copper grids using 2% methylcellulose in 2.3M sucrose, blocked with 1% BSA, and immunolabelled with anti-CD155 (Proteintech, 84138-1-RR) and anti-CD63 (Santa Cruz Biotechnology, sc-5275) antibodies. They were then incubated with gold-conjugated secondary antibodies (goat anti-rabbit, 6 nm, Aurion, 25104; goat anti-mouse, 15 nm, Aurion, 25133) and visualized using TEM following the aforementioned procedures.

The size distribution and concentration of the isolated EVs were quantified via nanoparticle tracking analysis (NanoSight NS300, Malvern Panalytical Instruments, UK).

## 2.10 | Deglycosylation of CD155

RIPA lysis buffer (Millipore, 20–188) supplemented with 1% protease inhibitor cocktail (Beyotime, P1005) was added to both H1975 cells and EVs isolated from H1975 cells and plasma. The samples were lysed on ice for 10 min, then centrifuged at 16,000 × g for 10 min at 4°C, and the supernatants were transferred to new tubes. Next, the samples were treated with either PNGase F (Novoprotein, PE011) or Endo H (Novoprotein, PE017) to deglycosylate CD155 according to the manufacturer's instructions. Finally, the samples were boiled with SDS–PAGE loading buffer for subsequent western blotting analysis.

## 2.11 | Western Blotting

The total protein content of cell lysates and EVs was quantified using a BCA protein assay kit (Beyotime Biotechnology, P0010) and separated on 10% SDS–PAGE gels (Sangon Biotech, C631100). The proteins were then transferred onto PVDF membranes (Millipore, IPVH00010). After transfer, the membranes were stained with Ponceau S (Sangon Biotech, C640005) to visualize whole protein as a normalization factor. The membranes were incubated with different primary antibodies, including anti-CD63 (Santa Cruz Biotechnology, sc-5275), anti-TSG101 (ABclonal, A5789), anti-Alix (ABclonal, A2215), anti-Syntenin-1 (Proteintech, 22399-1-AP), anti-Calnexin (ABclonal, A4846), anti-GRP94 (ABclonal, A26311), anti-CD155 (Sino Biological, 84138-5-RR), anti-GAPDH (Beyotime, AF2823), anti-albumin (Sino Biological, 68001-R101), anti-human IgG (Solarbio, SE101), anti-MVP (Proteintech, 16478-1-AP), anti-GYS1 (Abcam, ab40810), anti-SERPINA3 (Proteintech, 12192-1-AP), anti-HECTD3 (Proteintech, 11487-1-AP), anti-SERPING1 (Proteintech, 12259-1-AP), anti-TPM4 (Abcam, ab181085) and anti-APOD (Proteintech, 10520-1-AP). Subsequently, the membranes were incubated with HRP-conjugated goat anti-rabbit IgG (Sangon Biotech, D110058) or HRP-conjugated goat anti-mouse IgG (Sangon Biotech, D110087) for 60 min at room temperature. Blots were developed using an ECL Enhanced Kit (ABclonal, RM00021) and detected using an Amersham Imager 600 (GE Healthcare Life Science, USA).

## 2.12 | ELISA

The concentration of EV CD155 was measured using a CD155 ELISA Kit (CUSABIO, CSB-EL019093HU) following the manufacturer's instructions, with EV lysates as the input material.

## 2.13 | Flow Cytometry

On-beads flow cytometry of EVs was performed following a previously described method (Huang et al. 2018). Briefly, 20 µg EVs were attached to 10 µL 4 µm aldehyde/sulphate latex beads (Invitrogen, A37304). Subsequently, EVs-bound beads were incubated with APC anti-human CD63 (Biolegend, 353007) and FITC anti-human CD155 (Biolegend, 337627) or APC Mouse IgG1,  $\kappa$  isotype control (Biolegend, 400121) and FITC Mouse IgG1,  $\kappa$  isotype control (Biolegend, 400109) for 60 min at room temperature. All data were acquired and analysed using the BD FACSCalibur (BD Biosciences, FACS Aria III) and FlowJo software.

## 2.14 | In-Gel and In-Solution Digestion and Desalting

In-solution digestion was performed as previously described (Zhang et al. 2021). Briefly, 50 µg of total protein from EVs isolated from cell lines was lyophilized and resolubilized in lysis buffer (8 M urea/100 mM  $\text{NH}_4\text{HCO}_3$ ). Proteins were reduced using 20 mM dithiothreitol (Sigma–Aldrich, 43815) at 37°C for 90 min, followed by alkylation using 40 mM iodoacetamide (Sigma–Aldrich, I1149) for 45 min at room temperature in the dark. Subsequently, the samples were diluted in 50 mM  $\text{NH}_4\text{HCO}_3$  to lower the urea concentration to <2 M. Samples were digested overnight at 37°C using trypsin (Promega, V511C) at a trypsin-to-protein ratio of 1:50 (w/w).

In-gel digestion was performed as described previously (Chen et al. 2017). SDS–PAGE gels were cut into small pieces and destained with 50 mM triethylammonium bicarbonate in 40% acetonitrile. Gel dehydration was performed in 100% acetonitrile (ACN). Proteins were reduced using 5 mM Tris (2-carboxyethyl) phosphine, followed by alkylation with 10 mM methyl methanethiosulfonate. Digestion was performed overnight at 37°C with trypsin at a trypsin-to-protein ratio of 1:50 (w/w), and the reaction was quenched with formic acid (FA, 0.1%, v/v). All peptides were desalted using C18 ZipTip pipette tips (Millipore, ZTC18S008). Peptides were eluted in 40 µL of 40% ACN/0.1% FA and 40 µL of 60% ACN/0.1% FA, and the eluted peptide solutions were combined and lyophilized.

## 2.15 | Data-Independent Acquisition (DIA)–MS Data Acquisition

All nanoLC–MS/MS experiments were performed on Orbitrap Eclipse (Thermo Fisher Scientific) equipped with an Easy-nLC 1200 HPLC system (Thermo Fisher Scientific). The peptides were loaded on a trap column (100 µm × 2 cm) packed with Reprosil-Pur C18 5 µm particles and then separated on an analytical column (75 µm × 25 cm) with Reprosil-Pur C18 3 µm particles (Dr. Maisch GmbH).

The peptides bound to the column were eluted with a 103-min linear gradient using mobile phase A (0.1% FA in water) and mobile phase B (0.1% FA in acetonitrile) as follows: 5%–8% B for 8 min, 8%–22% B for 50 min, 22%–32% B for 12 min, 32%–95% B for

1 min, and maintained at 95% B for the final 7 min, at a flow rate of 300 nL/min.

MS analysis was performed using an Orbitrap Eclipse mass spectrometer (Thermo Fisher Scientific). In DIA mode, the MS data were acquired at a high resolution of 120,000 ( $m/z$  200) across the mass range of 400–1210  $m/z$ . The target value was  $4.00\text{E} + 05$ , with a maximum injection time of 50 ms. One full scan was followed by 40 windows with an isolation width of 16  $m/z$  for fragmentation in the ion-routing multipole with an HCD-normalized collision energy of 30%. MS/MS spectra were acquired at a resolution of 30,000 at  $m/z$  200 in the mass range of 200–2000  $m/z$ . The target value was  $4.00\text{E} + 05$ , with a maximum injection time of 50 ms. For the nano-electrospray ion source setting, the spray voltage was 2.0 kV with no sheath gas flow and a heated capillary temperature of 320°C.

## 2.16 | DIA Data Analysis

The DIA raw data from Orbitrap Eclipse were analysed using Spectronaut version 18 (Biognosys) with the “DirectDIA” mode for protein identification and quantification. The UniProt human protein database (updated on November 2022) was used to search for data from the EVs samples. The most important searching parameters were set as the default, as follows: trypsin as the enzyme, with two missed cleavages allowed for searching; mass tolerance of the precursor set as 10 ppm and the product ion tolerance at 0.02 Da; cysteine carbamidomethylation as a fixed modification; and methionine oxidation as a variable modification. The false discovery rate (FDR) was set to 1% for both protein and peptide identifications. The data were filtered by  $q$ -value, and the “Global Normalization” was set as “Median” with enabled cross-run normalization.

## 2.17 | Spectral Library Construction and PRM Analysis

The SpectroDive 11.12 software (Biognosys, Switzerland) was used for PRM analysis (Li et al. 2023). To develop the PRM assay, all raw DIA data were searched using the Pulsar engine against the human SwissProt FASTA database (20,601 entries) for spectral library generation. Other search parameters were set as follows: enzyme was selected as trypsin/P; carbamidomethyl (C) as a fixed modification, whereas acetyl (Protein N-term) and oxidation (M) were set as variable modifications; ion types b and y; and other settings were set as default. The top 100 DEPs including CD155 identified in the discovery cohort were selected for the following settings for the assay panel generation: precursor  $m/z$ , 350–1500; precursor charge, 2–3; missed cleavages, 0; peptide length, 8–25; only proteotypic; allowed modification, carbamidomethyl (C); fragment  $m/z$ , 300–1800; max fragment charge, 2; ion types, b and y; min fragment length, 3; and top N fragments, 6. The PRM analysis was performed using an Orbitrap Eclipse (Thermo Fisher Scientific) equipped with an Easy-nLC 1200 HPLC system (Thermo Fisher Scientific). Peptides from each sample were equally mixed together, and 1 µg of the mixed peptides spiked with 10× iRT standard peptides were used for unscheduled PRM MS/MS analysis. Full MS scans were acquired at a resolution of 60,000 at  $m/z$  200 across the mass range of 350–1200  $m/z$

with an AGC of 6e5 and a maximum injection time of 50 ms. MS/MS spectra were acquired at a resolution of 30,000 at  $m/z$  200, an isolation window of 1, a collision energy of 30%, and an AGC target value of 2E5 with a maximum injection time of 80 ms. We discarded precursors with poor signal and peak shapes based on the results of the unscheduled PRM. After retention time calibration, the precursors of the proteins to be targeted were selected for the modified PRM panel and the scheduled method generation. The retention time window was set for  $\pm 3$  min. For PRM assay development and data analysis, a  $q$ -value cutoff of 0.01 was set for peptide selection. All selected peaks were manually checked after automated peak detection using SpectroDive. Product ion signal peaks with significant interfering signals around the peak apex were excluded, and more than three transitions per precursor were selected for quantification using SpectroDive.

## 2.18 | Bioinformatics and Statistical Analysis

CD155 RNA expression data and primary tumour size (T stage) were obtained from The Cancer Genome Atlas (TCGA) NSCLC cohort. RNA expression values were normalized to transcripts per million. Cases lacking T stage or RNA expression data were excluded from the analysis. Patients were stratified into high (top 25%) and low (bottom 25%) CD155 expression groups based on RNA levels. Differences in T stage between the groups were assessed using Chi-square test, with statistical significance set at  $p < 0.05$ .

Protein abundance data were imputed with the sequential k-nearest neighbours algorithm for missing values, followed by ASINH-transformed to normalize the values and enable a more robust comparison between the two groups. The transformed data were visualized using statistical plots, including heatmaps and violin plots. For DEPs analysis, a two-sample  $t$ -test was performed on the protein abundance data. A  $p$  value of 0.05 was considered statistically significant ( $*p < 0.05$ ,  $**p < 0.01$ ,  $***p < 0.001$  and  $****p < 0.0001$ ). For the proteomics of EVs from cell lines, proteins with a Log2 fold change (FC)  $> 1.5$  or  $< -1.5$  were considered upregulated or downregulated proteins, respectively. For the proteomics of immunocaptured EVs from plasma, proteins with a Log2 FC  $> 1.0$  or  $< -1.0$  were considered upregulated or downregulated, respectively. ROC curve analysis was performed using the R package pROC for statistical assessment. For targeted proteomics, normalization was performed using the total ionic chromatography signal from MS1. The R packages glmnet, random forest, and Boruta were used for the feature selection.

## 3 | Results

### 3.1 | Characterization of EVs Isolated From NSCLC Cell Lines and the Plasma of Patients

EVs were isolated from cell culture supernatants and plasma via ultracentrifugation. TEM images revealed the characteristic cup-shaped morphology of the EVs, with sizes ranging from 60 to 200 nm (Figure 1A). The average diameters of EVs from cell culture supernatants and plasma were determined to be  $128.9 \pm 1.9$

and  $163.2 \pm 8.6$  nm, respectively, using nanoparticle tracking analysis, with the peak diameters being 120.5 and 159.8 nm, respectively (Figure 1B). Western blotting results confirmed the presence of the positive EV markers CD63, TSG101, Alix and Syntenin-1, whereas the negative EV markers (Calnexin and GRP94) were absent (Figure 1C). These results confirmed the successful isolation of EVs from both cell culture supernatants and plasma samples.

### 3.2 | Proteomic Profiling of EVs Isolated From NSCLC Cell Lines Using DIA Mass Spectrometry

Untargeted proteomic analyses were performed on EVs isolated from NSCLC cell lines (NSCLC-EVs) and human bronchial epithelial cell lines (control-EVs) for the proteomic characterization of EVs from NSCLC, and the proteomic data were processed using multivariate statistical techniques. The principal component analysis (PCA) revealed clear distinctions between the NSCLC and control groups, indicating significant differences in protein expression profiles (Figure 2A). The Venn diagrams presented in Figures 2B,C and S1A revealed 4874, 2912, 4537, 3271 and 4561 proteins in NSCLC-EVs, A549-EVs, H1975-EVs, H460-EVs and SK-MES-1-EVs, respectively. Meanwhile, 3633, 3291, 3447 and 2784 proteins were identified in control-EVs, BEAS-2B-EVs, BEP2-D-EVs and HPAEpiC-EVs, respectively. Additionally, 4355 and 3289 proteins in NSCLC-EVs and control-EVs, respectively, are previously recorded in the Vesiclepedia database (Kalra et al. 2012). The raw proteomic results of the EVs isolated from each cell line sample, including protein identifiers, abundance levels and annotations, are provided in Table S2.

We analysed the fold change and significance of protein abundance using univariate statistical tests to identify DEPs between NSCLC-EVs and control-EVs. We identified 257 DEPs, with 139 and 118 showing higher and lower abundances in NSCLC-EVs, respectively (Table S3), as visualized in volcano plots (Figure 2D).

A heatmap generated using hierarchical clustering analysis highlighted the top 30 proteins with the most significant differences in expression (Figure 2E). Furthermore, 128 and 18 proteins were exclusively detected in NSCLC-EVs and control-EVs, respectively (Table S4). The 15 most abundant proteins in each group are presented in Figure 2F. Among the identified DEPs, we focused on CD155, a transmembrane glycoprotein that is significantly overexpressed in various cancers and is strongly associated with tumour progression and immune evasion (Liu et al. 2021; Freed-Pastor et al. 2021; Jin et al. 2022). Notably, CD155 was exclusively detected in NSCLC-EVs while absent in control-EVs, suggesting its potential as a marker for capturing TDEVs.

### 3.3 | Elevated CD155 Expression in EVs Derived From NSCLC Cells and the Plasma of Patients

To determine whether CD155 could serve as a potential tumour biomarker, we quantified its expression in EVs and NSCLC tissues, and then evaluated its association with disease progression. We assessed CD155 expression in NSCLC-derived EVs and cells to understand its role in NSCLC-EVs. CD155 was exclusively detected in NSCLC-EVs compared with the control-EVs using

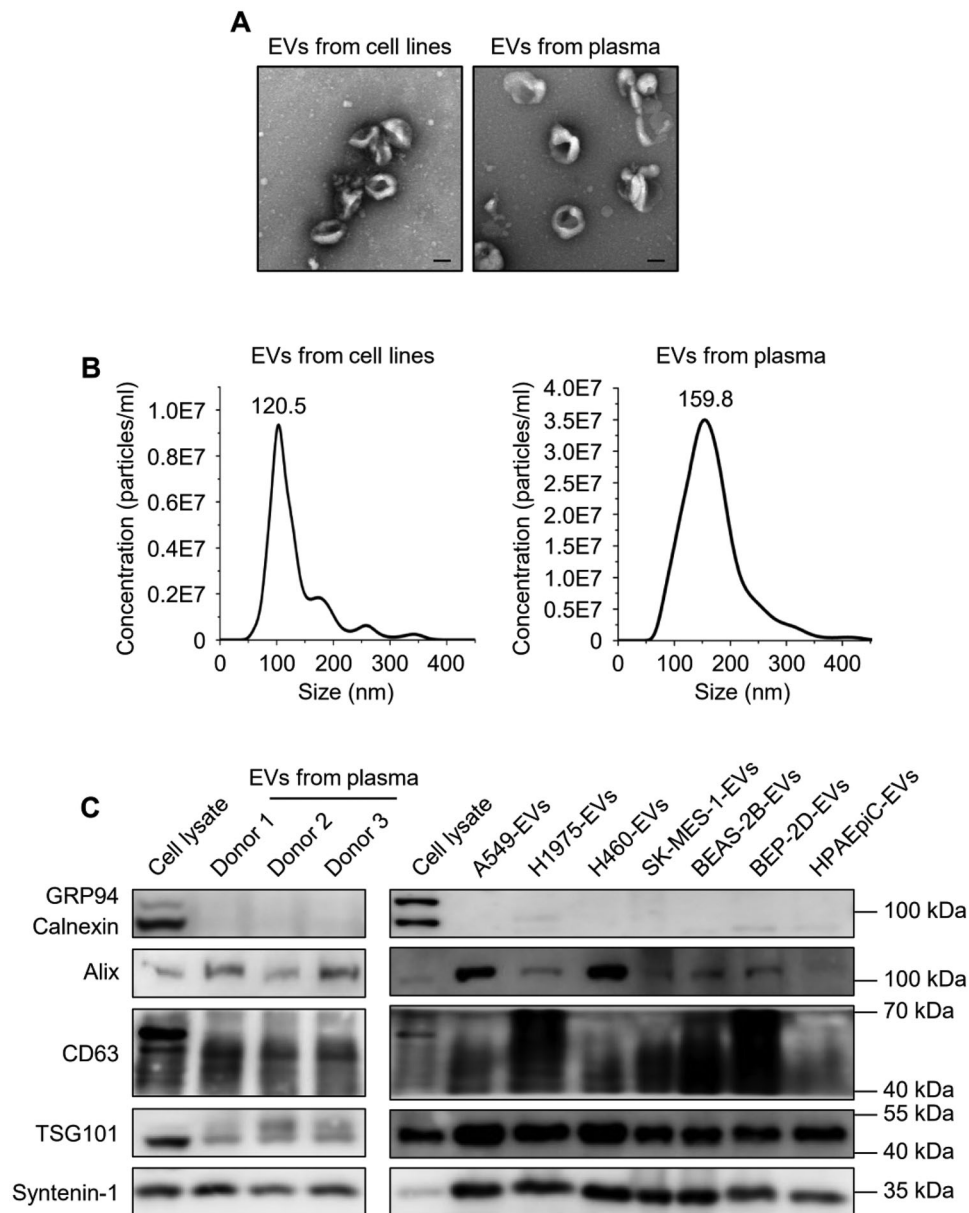


**FIGURE 1** | Characterization of EVs derived from cell lines and clinical plasma. (A) Representative TEM images of purified EVs. Scaled bars: 100 nm. Left: EVs derived from cell culture supernatant. Right: EVs isolated from plasma. (B) Analysis of the size distribution and concentrations of isolated EVs using nanoparticle tracking analysis. Left: EVs isolated from cell culture supernatant. Right: EVs isolated from plasma. (C) EV biomarker detection using western blotting.

western blotting and flow cytometry (Figure 3A,B). In addition, Western blotting analysis of cell lysates confirmed significantly higher CD155 expression in NSCLC cells compared to control cells (Figure S2A).

Next, we evaluated CD155 levels in plasma-derived EV lysates and EV-depleted plasma to differentiate EV-associated CD155 from its soluble form. We observed that CD155 was not only present in EVs (Figure S2B) but also significantly elevated in EV lysates from NSCLC patients compared to healthy individuals (Figure 3C–E). Receiver operating characteristic (ROC) curve analysis showed an area under the curve (AUC) of 0.872 for EV CD155 in distinguishing patients with NSCLC from healthy individuals (Figure 3F). Additionally, a significant correlation was

observed between CD155 levels in plasma EVs and the maximum tumour diameter ( $p = 0.0079$ , Figure 3G).

In addition, we examined CD155 expression in NSCLC tissue microarrays using immunohistochemistry (IHC). CD155 was specifically localized on the tumour cell membrane, whereas adjacent normal cells exhibited undetectable CD155 levels. Quantitative analysis of IHC staining intensity indicated an association between elevated CD155 levels and advanced disease stages (Figure 3H).

To further elucidate the role of CD155 in tumour progression, we conducted both in vitro functional assays and analyses of clinical data from the TCGA NSCLC cohort. It was revealed

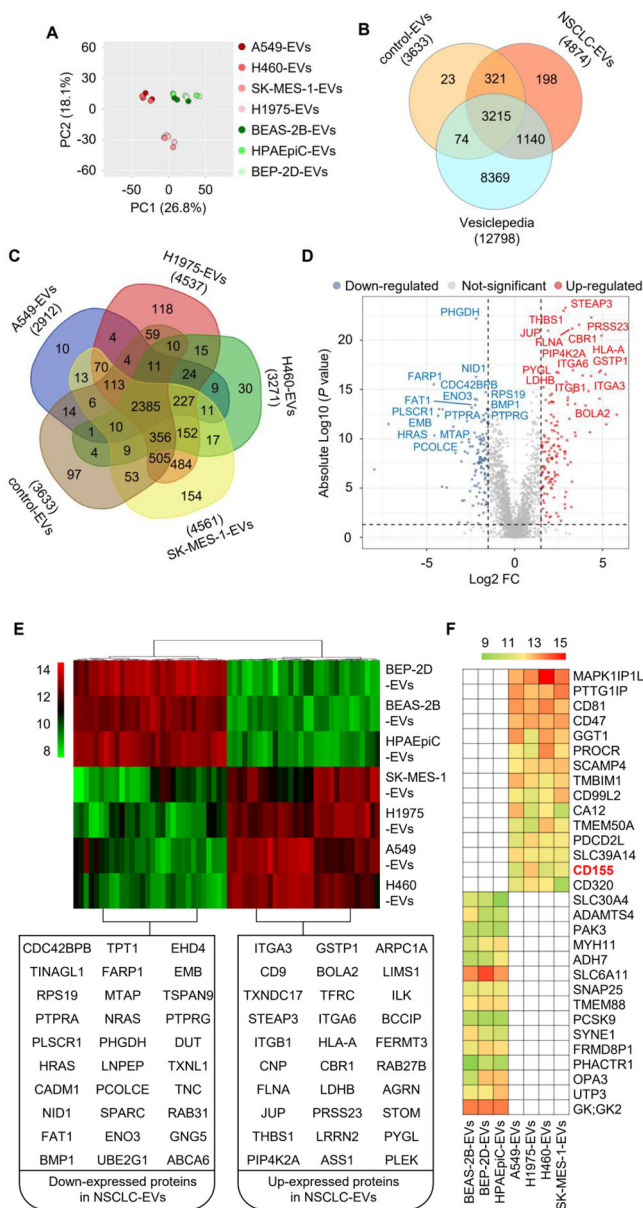


**FIGURE 2 |** Proteomic profiling of EVs isolated from NSCLC and control cell lines using DIA mass spectrometry. (A) PCA of the protein profiles of NSCLC-EVs and control-EVs. (B) Venn diagram showing the identified proteins in NSCLC-EVs and control-EVs. (C) Venn diagram showing the identified EV proteins in each sample of NSCLC and control groups. (D) Volcano plots representing the differences in protein expression between NSCLC-EVs and control-EVs. (E) Heatmap showing hierarchical clustering of the top 30 proteins with the most significant differences in expression between EVs from NSCLC and control cell lines. The colour scale represents normalized protein expression levels. (F) Heatmap displaying the 15 most abundant proteins exclusively detected in NSCLC-EVs (top) and control-EVs (bottom). The colour scale represents the relative abundance of these proteins, white indicating proteins that were not detected.

that CD155-overexpressing H1975 cells exhibited significantly enhanced proliferative capacity compared to wild-type cells, while CD155-knockout H1975 cells showed markedly suppressed proliferation (Figure S2C). Furthermore, we analysed CD155 RNA expression and T stage data from the TCGA NSCLC cohort. It can be observed that patients with high CD155 expression (top

25% of expression values) had significantly larger tumour volumes compared to those with low expression (bottom 25%,  $p = 0.0002$ , Figure S2D). Taken together, these findings suggested that CD155 may serve as a potential indicator of tumour aggressiveness.

### 3.4 | CD155 Localized on EV Membrane and Originated From the Cell Surface

Considering CD155 is a transmembrane protein, we hypothesized that EV CD155 primarily originates from the cell surface. To test this hypothesis, we examined the co-localization of CD155 with CD63 (a marker of multivesicular bodies), Rab5 (a marker of early endosomes) and Rab7 (a marker of late endosomes) using immunofluorescence. As shown in Figure 4A,B, CD155 was predominantly localized on the cell membrane and exhibited greater co-localization with CD63 and Rab5 than with Rab7, suggesting its involvement in endosome maturation. Since cargos directly from the endoplasmic reticulum and Golgi are packaged into EVs as the endosome matures (van Niel et al. 2018), we further investigated whether EV CD155 originates from these organelles by taking advantage of its glycosylation (Zibert and Wimmer 1992; Stanley 2011). As shown in Figure 4C, treatment with PNGase F effectively removed the oligosaccharide chains of CD155, whereas these chains were resistant to Endo H cleavage, indicating that EV CD155 does not derive directly from the endoplasmic reticulum or early Golgi. In addition, in EVs derived from H1975 cells, CD155 was clearly localized on the EV membrane, whereas it was not observed in EVs from BEAS-2B cells (Figure 4D). As demonstrated in Figure 4E, EVs containing CD63 and CD155 immunocaptured with antibodies were confirmed by western blotting. Moreover, the iEM images further confirmed that CD155 is localized on the EV membrane rather than within the lumen of EVs isolated from plasma (Figure 4F). Collectively, these findings demonstrated that CD155 localizes on EV membrane and is derived from the cell surface, prompting us to apply a similar strategy to isolate potential CD155+ TDEVs from the total plasma EVs for further analysis.

### 3.5 | Proteomic Profiling of CD155+ TDEVs From the Plasma of Patients With NSCLC Using DIA Mass Spectrometry

Considering that CD155 is selectively overexpressed in cancer cells and is localized on the EV membrane, we further investigated the proteomic profiles of CD155+ TDEVs. To obtain high-quality CD155+ TDEVs, we first isolated total EVs from pooled plasma samples using differential ultracentrifugation. We then removed immunoglobulins (Igs) and albumin (ALB) using immunoprecipitation to eliminate high-abundance protein contamination from plasma (Figure S3A). A substantial quantity of CD155+ TDEVs were detected in the EVs of the patients with NSCLC (Figure 5A). In contrast, CD155+ TDEVs were not detected in the EVs from the healthy control group.

After purifying the immunocaptured EVs, we identified 2021 and 2234 proteins in the NSCLC and healthy control groups, respectively, using quantitative proteomic analysis of the 12 EV samples (Figure 5B). Notably, we identified 281 DEPs in CD155+ TDEVs, with 126 and 155 showing higher and lower abundances,

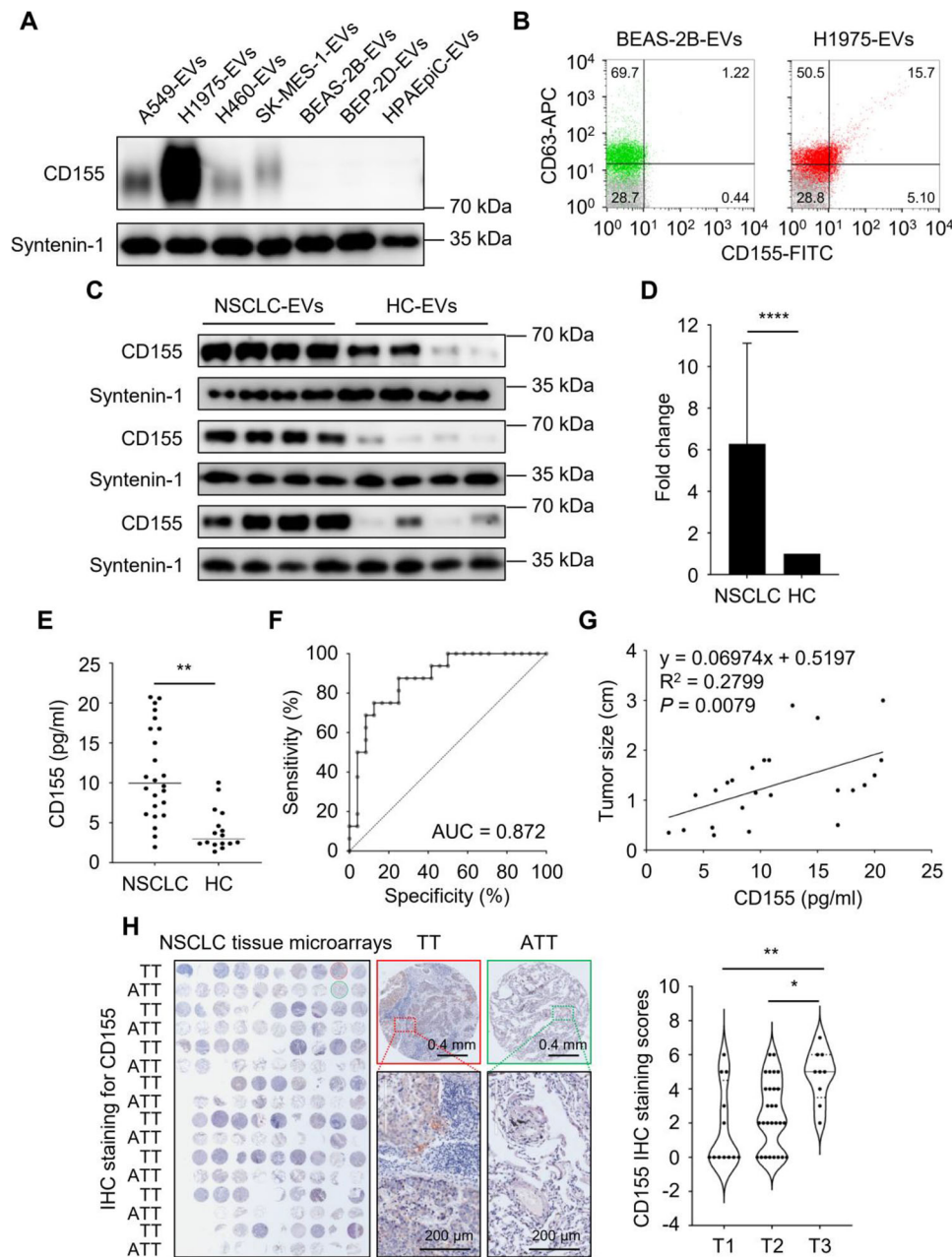


**FIGURE 3** | Elevated CD155 expression in EVs from NSCLC cells and patient plasma compared with healthy individuals. (A) Western blotting analysis of CD155 in EVs isolated from NSCLC and control cell lines. (B) Flow cytometry analysis of CD155 and CD63 in EVs isolated from H1975 and BEAS-2B cells. (C) Western blotting analysis of CD155 abundance in EVs from the plasma of patients with NSCLC and healthy individuals in three independent tests. (D) Quantitative assessment of the fold change in CD155 expression from panel C, normalized to whole protein. (E) CD155 expression in EVs isolated from plasma of patients with NSCLC (LUAD,  $n = 20$ ; LUSC,  $n = 4$ ) and healthy individuals ( $n = 16$ ) using ELISA. (F) ROC curve analysis of the diagnostic potential of EV-CD155 in distinguishing patients with NSCLC from healthy individuals. (G) Pearson correlation analysis of CD155 expression in EVs and tumour size in patients with NSCLC ( $n = 24$ ). (H) IHC analysis for CD155 expression in NSCLC tissue microarrays. Left: IHC staining images of paired tumour tissues (TT) and adjacent tumour tissues (ATT) ( $n = 35$ ). Right: quantitative analysis of IHC intensity for CD155 ( $n = 49$ ). T1, T2, and T3 in the quantification data refer to the tumour stages defined by the TNM classification system of NSCLC.

respectively (Table S4). Detailed raw proteomic data, including protein identifiers and abundance levels, are available in Table S5, while the full list of DEPs with fold changes and  $p$  values are presented in Table S6. As detailed in Table S5, CD155 was consistently identified in CD155+ TDEVs. In contrast, CD155 was detected in only one out of seven CD63+ HC-EVs, and its abundance in this sample was significantly lower than in CD155+

TDEVs. PCA and hierarchical clustering of these DEPs effectively differentiated patients with NSCLC from healthy individuals (Figures 5C and S3B). Volcano plots clearly showed significant differences in protein expression between the NSCLC and healthy control groups (Figure 5D). The 50 most important proteins ranked by the random forest algorithm for the classification of the two groups are presented in Figure 5E.

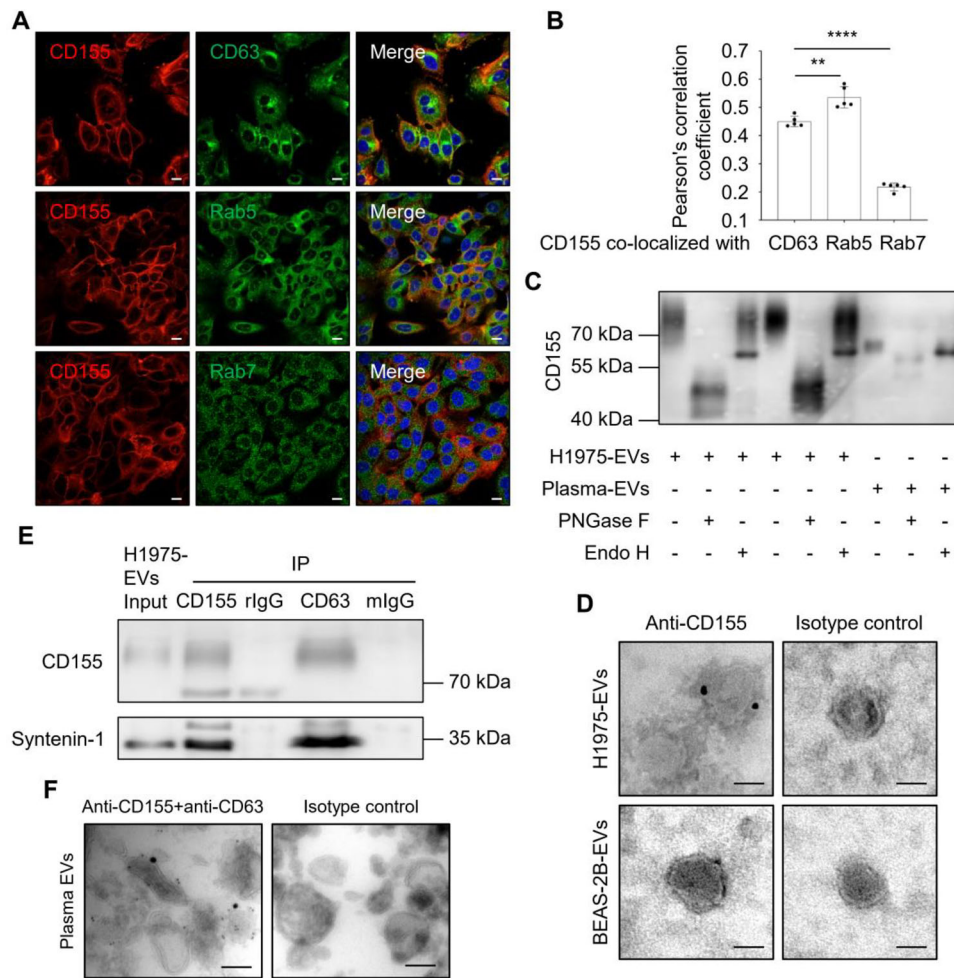


**FIGURE 4** | Cellular origin and membrane localization of CD155 in EVs. (A) Immunofluorescence analysis of H1975 cells showing CD155 displayed higher co-localization with CD63 and Rab5 than Rab7. Nuclei were stained with DAPI. Scale bars: 10  $\mu$ m. (B) Quantitative analysis of Pearson's correlation coefficients demonstrating the co-localization between CD155 with CD63, Rab5, and Rab7 in H1975 cells. (C) Western blotting analysis of cellular and EV CD155 treated with different endoglycosidases. PNGase F effectively removes the oligosaccharide chains of CD155, whereas these chains are resistant to Endo H cleavage. (D) Representative iEM images of EVs isolated from H1975 and BEAS-2B cells. EVs were stained with anti-CD155 antibodies. Scale bars: 100 nm. (E) Western blotting analysis of the immunocaptured EVs derived from H1975 cells using antibody against CD63 or CD155. (F) Representative iEM images of plasma EVs demonstrating CD155 localized on the EV membrane rather than within the lumen. Scale bars: 100 nm.

### 3.6 | Determination of EV Biomarker Candidates in the Verification Cohort

To validate whether the identified differential proteins from the discovery cohort could serve as potential biomarkers, a total of 89 tryptic peptides derived from 51 proteins were subjected to targeted proteomics using PRM in 71 individual samples (LUAD,  $n = 29$ ; LUSC,  $n = 9$ ; healthy individuals,  $n = 33$ ). Notably, 49 proteins were successfully quantified, of which 21 exhibited statistically significant differences between the NSCLC and healthy control groups (Figure 6A, Table S7). To ensure robust and comprehensive biomarker selection, we utilized three complementary machine learning algorithms: LASSO regression for feature selection, random forest for ranking feature importance, and Boruta for identifying statistically significant features. The combination containing MVP, GYS1, SERPINA3, SERPING1, CP, IGLL1 and APOD from the 21 DEPs was selected using LASSO (penalized coefficients,  $\lambda = 0.07$ ) (Figure 6B). The importance of the classification of the two groups of the 21 DEPs

ranked by random forest and Boruta is shown in Figure 6C,D. To identify the optimal biomarker combination, we tested the feature variables from the three algorithms using a confusion matrix, evaluating diagnostic performance and excluding variables that did not enhance sensitivity or specificity. Notably, a panel of seven proteins—MVP, GYS1, SERPINA3, HECTD3, SERPING1, TPM4 and APOD—demonstrated good performance with 92.3% sensitivity and 88.9% specificity in the confusion matrix (Figure 6E). Interestingly, a panel of 21 DEPs exhibited 76.9% sensitivity and 77.8% specificity. Furthermore, western blotting results demonstrated significant differences in the expressions of these candidate biomarkers (MVP, GYS1, SERPINA3, HECTD3, SERPING1 and TPM4) in plasma EVs from patients with NSCLC and healthy individuals (Figure 6F,G). Furthermore, this panel of seven biomarkers in the ROC curve analysis achieved an AUC of 1.0 with 100% sensitivity and specificity based on targeted proteomics data (Figure 6H). Finally, the PCA results demonstrated that this panel effectively discriminated patients with NSCLC from healthy individuals better than the set of 21 DEPs (Figure 6I).

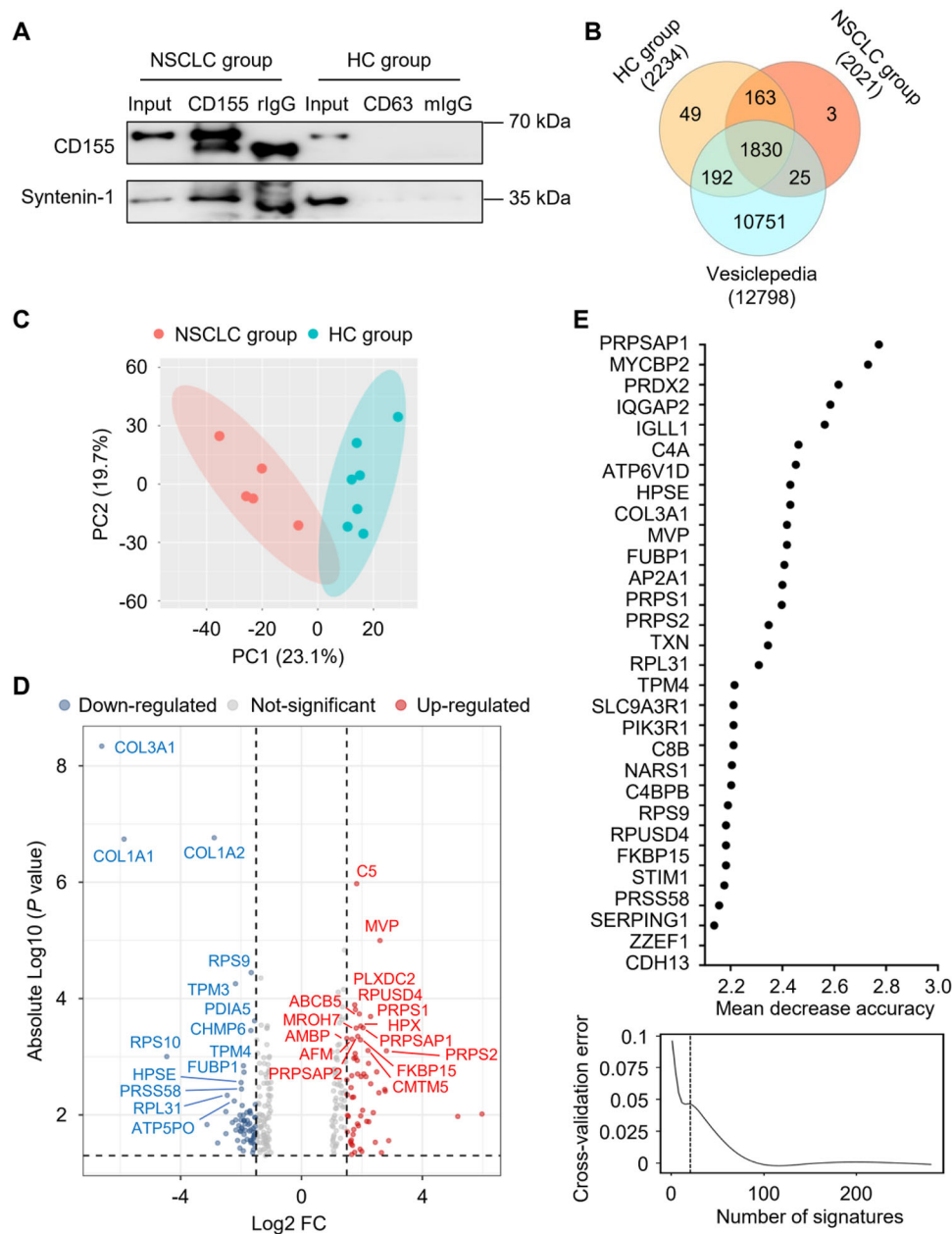


**FIGURE 5** | DIA proteomic profiling of immunocaptured EVs from plasma of patients with NSCLC and healthy control groups. (A) Western blotting analysis of the immunocaptured EVs from the total plasma EVs from patients with NSCLC and healthy control groups. (B) Venn diagram showing the identified proteins in immunocaptured EVs from the two groups. (C) PCA results of the identified proteins in immunocaptured EVs from NSCLC and healthy control groups. (D) Volcano plots demonstrating the significant differences in protein expression of immunocaptured EVs from NSCLC and healthy control groups. (E) The top 50 important proteins identified using the random forest algorithm.

Collectively, these findings indicated the promising potential of this panel for NSCLC screening.

## 4 | Discussion

This study aimed to identify potential biomarker-based TDEVs for liquid biopsy in NSCLC by characterizing tumour biomarkers in TDEVs to effectively distinguish them from normal cell-derived EVs in body fluids. Comparative proteomic analysis of samples from patients with cancer and healthy individuals revealed significant upregulation of CD155 in the plasma EVs of patients

with NSCLC. Using CD155 as a bait to enrich CD155+ TDEVs was a crucial step in this study.

Previous studies have reported significantly higher CD155 expression in various tumours compared with the low or undetectable levels in most healthy tissues (Zhan et al. 2022; Brlic et al. 2019). CD155 regulates multiple cellular functions, including adhesion, contact inhibition, migration, proliferation, and immune responses (Wang et al. 2022; Zhou et al. 2023). Notably, blocking CD155 interaction with its inhibitory receptors enhances the antitumor activity, suggesting its potential as a therapeutic target (Zhou et al. 2024; Chiang and Mellman 2022). Importantly,

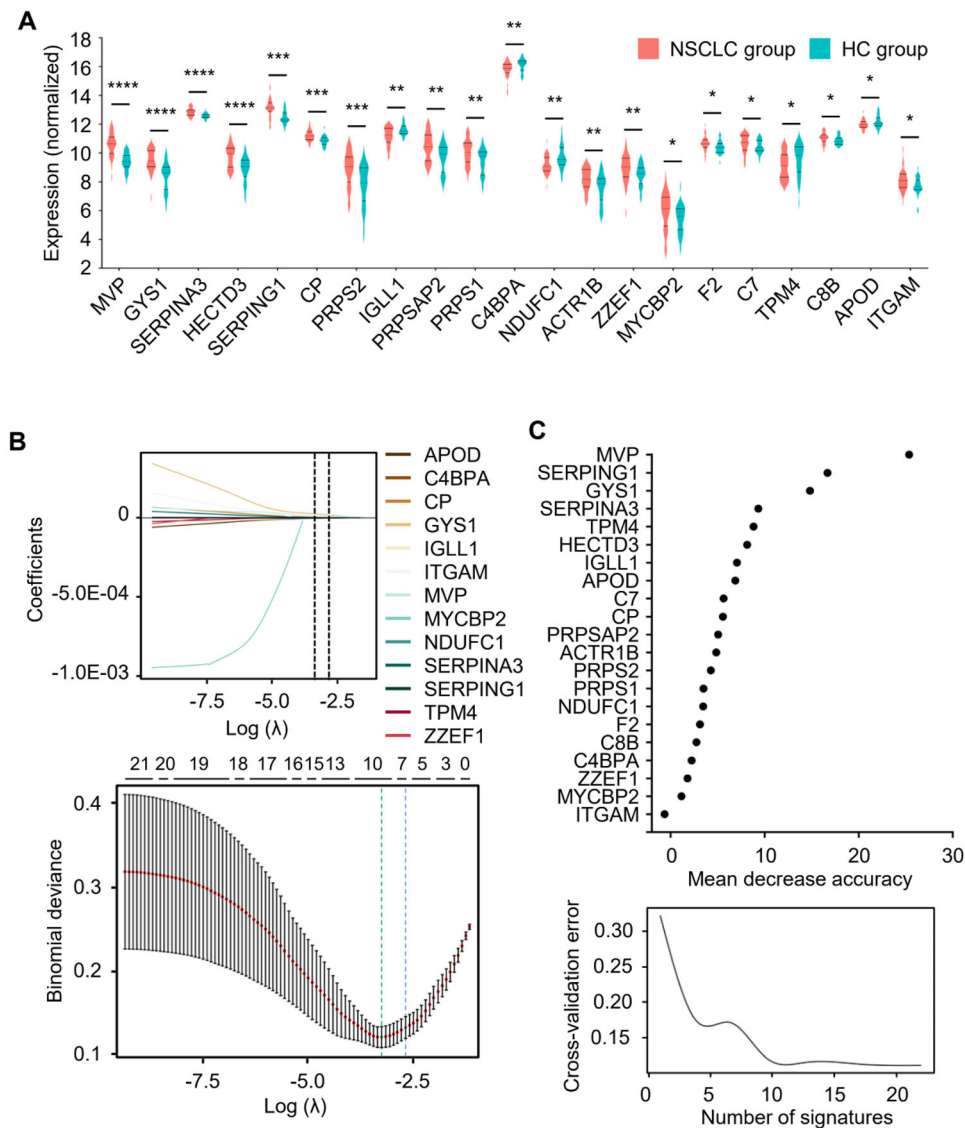


**FIGURE 6** | Identification and evaluation of the candidate biomarkers in EVs for NSCLC screening. (A) Violin plots showing the abundance of the 21 DEPs in EVs between NSCLC patients and healthy individuals. (B) Feature selection from the 21 DEPs using LASSO regression. (C) Random forest algorithm evaluating the importance of the 21 DEPs in the classification of NSCLC patients and healthy individuals. (D) Boruta algorithm evaluating the importance of the 21 DEPs in the classification of NSCLC patients and healthy individuals. (E) Confusion matrix showing the classification of the two groups with the selected 7- and 21-protein panels. (F) Western blotting analysis of the expression of seven biomarkers in the plasma EVs (LUAD,  $n = 16$ ; LUSC,  $n = 4$ ; healthy individuals,  $n = 22$ ). (G) Statistical analysis of the relative expressions of the seven biomarkers from panel G, normalized to whole protein. Dashed lines, black dots, and grey dots represent  $p = 0.05$ ,  $p < 0.05$  and  $p > 0.05$ , respectively. (H) ROC curve analysis of the panel of seven proteins in distinguishing between NSCLC patients and healthy individuals. (I) The classification of NSCLC patients and healthy individuals based on the panel of 7 and the panel of 21 DEPs using PCA.

the surface localization of CD155 confers distinct advantages over luminal EV proteins, making it particularly suitable for downstream applications such as liquid biopsy and targeted therapies. In this study, CD155 was rarely detected in EVs from the plasma of healthy individuals but was significantly higher in the EVs from the patients with NSCLC. CD155+ TDEVs were immunocaptured from the total EVs of patients with NSCLC. Notably, compared with unpurified EVs (Figure S4), the PCA results of the purified EVs demonstrated a better separation between the NSCLC and healthy control groups. These results indicated that CD155+ TDEVs were derived from TDEVs. Similar protocols were reported using magnetic beads coated with A33

and EpCAM antibodies to immunocapture EVs from LIM1863 cells revealed distinct protein profiles (Mathivanan et al. 2010; Tauro et al. 2013), and obtaining tumour-related biomarkers in plasma EVs of chronic lymphocytic leukaemia and colon cancer patients through immunoaffinity separation of EpCAM+ EVs (Belov et al. 2016; Ostensfeld et al. 2016).

In this study, we identified 281 and 21 DEPs in the discovery and verification cohorts, respectively. We then used machine-learning-based feature selection to select biomarkers from our high-dimensional proteomic data. Using LASSO regression, we identified a biomarker combination, including MVP, GYS1,

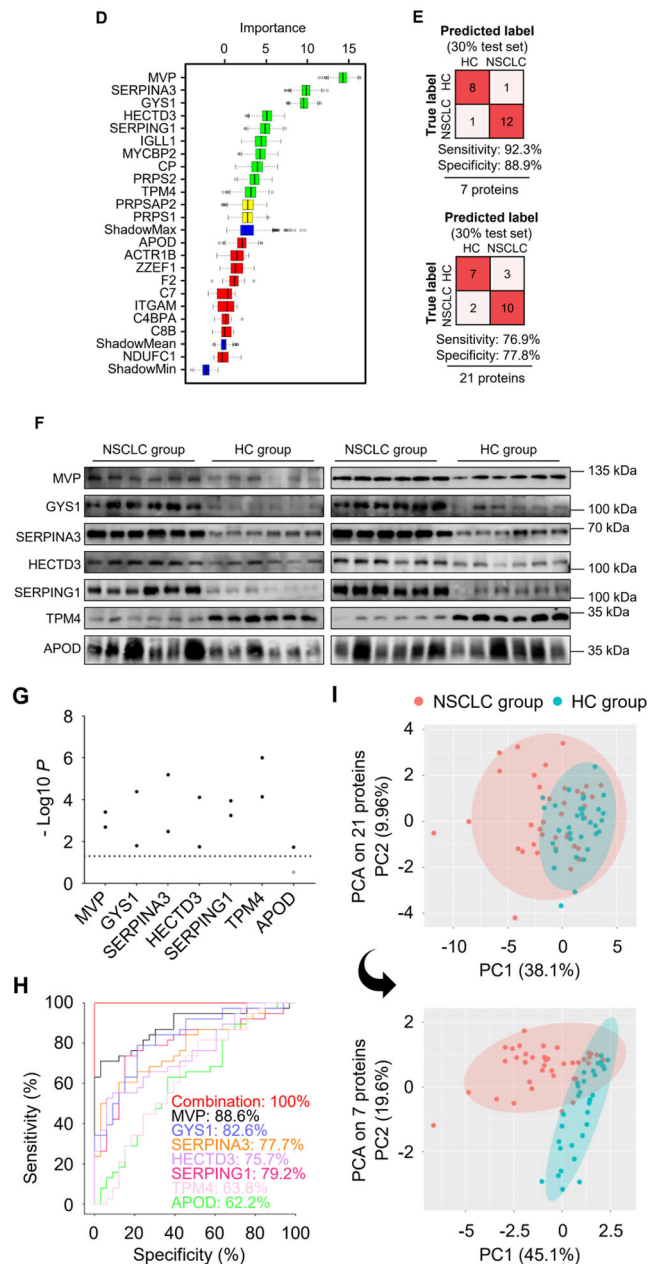


**FIGURE 6** | (Continued)

SERPINA3, SERPING1, CP, IGLL1 and APOD. However, this combination demonstrated 76.9% sensitivity and 77.8% specificity in the test set. In addition, the combination of the top seven important proteins—MVP, GYS1, SERPINA3, HECTD3, SERPING1, TPM4 and IGLL1—selected using the random forest algorithm did not improve diagnostic performance. The Boruta algorithm identified 10 important variables, including MVP, GYS1, SERPINA3, HECTD3, SERPING1, TPM4, IGLL1, MYCBP2, CP and PRPS2, with 69.2% sensitivity and 88.9% specificity. We then individually tested feature variables from the three algorithms using a confusion matrix algorithm to determine the optimal biomarker combination. Consequently, feature variables, including IGLL1, CP, MYCBP2 and PRPS2, which did not improve diagnostic performance, were excluded from the diagnostic panel. Notably, a diagnostic panel formed by a single algorithm or the intersection of important variables may not exhibit opti-

mal performance. Consequently, the feature variables from the three algorithms were comprehensively analysed to develop the most effective diagnostic panel. Finally, the panel comprising MVP, GYS1, SERPINA3, HECTD3, SERPING1, TPM4 and APOD achieved an AUC of 1.0 with 100% sensitivity and specificity in ROC curve analysis to distinguish patients with NSCLC from healthy individuals. Additionally, this panel demonstrated 92.3% sensitivity and 88.9% specificity in confusion matrix analysis.

Effective biomarkers must exhibit a significant statistical correlation with disease and pathophysiological relevance, facilitating the analysis of disease progression and serving as potential therapeutic targets (Karsdal et al. 2009; Jain and Jain 2010). In this study, the biomarker panel included MVP, GYS1, SERPINA3, HECTD3, SERPING1, TPM4 and APOD. MVP, a non-ATP-dependent transport protein associated with drug

resistance, is significantly upregulated in NSCLC, and its activation by chemotherapeutic drugs leads to chemotherapy resistance through multiple mechanisms, thus indicating its close association with NSCLC progression (Scheffer et al. 1995; Scheffer et al. 2000; Lou et al. 2021). GYS1, which is associated with a poor prognosis in NSCLC, is upregulated in irradiated A549 cells. Silencing GYS1 inhibits A549 proliferation but enhances resistance to radiotherapy, indicating its role as a rate-limiting enzyme in glycogen synthesis, thus affecting NSCLC metabolic reprogramming. This results in glycogen accumulation in tumour cells and enhances their survival under immune pressure and anticancer therapy (Giatromanolaki et al. 2017; Tsolou et al. 2023). Additionally, GYS1 expression in lung cancer cells is positively correlated with CCL5 and CSF1 and promotes M2-polarization of tumour-associated macrophages, facilitating tumour progression (Zhang et al. 2024; Kawamura et al. 2009; Li et al. 2020). SERPINA3 promotes tumour progression through inflammation-mediated angiogenesis, anti-apoptosis, tumour microenvironment remodelling, and immune suppression (Xing et al. 2021; Hulmi et al. 2020; Yuan et al. 2021). Serum biomarker panels containing SERPINA3 distinguish between patients with NSCLC and healthy individuals with AUCs of 0.85 and 0.77, respectively, with significant upregulation in NSCLC (Mehan et al. 2014; Jung et al. 2017). HECTD3 is overexpressed in various tumours, regulates apoptosis, and promotes tumour progression by modifying multiple proteins. It also enhances polyubiquitination of MALT1, caspase-8, caspase-9, and c-Myc to promote cancer progression (Li et al. 2013; Li et al. 2013; Zhang et al. 2022; Li et al. 2017). SERPING1, a complement regulator, is overexpressed in various tumours (Roumenina et al. 2019), and spatial transcriptomics of NSCLC brain metastases revealed significantly high SERPING1 expression associated with a poor prognosis (Zhang et al. 2022). In lung cancer, TPM4 promotes cell migration by enhancing F-actin assembly (Zhao et al. 2019). In esophageal squamous cell carcinoma (ESCC), TPM4 enhances cell identity confusion and promotes ESCC aggressiveness through the JAK/STAT/SOX2 pathway (Pan et al. 2022). Contrarily, TPM4 acts as a tumour suppressor in cervical and colon cancers (Luo et al. 2022; Yang et al. 2018). APOD expression trends also differ across cancer types, with downregulation in liver cancer and colon cancer and upregulation in gastric cancer and malignant melanoma, correlating with a poor prognosis (Miranda et al. 2003; Wang et al. 2024; Dong et al. 2023). In contrast, APOD downregulation was reported in exosomes from intraductal papillary mucinous neoplasms (Marin et al. 2023). In the discovery cohort of this study, APOD was upregulated in the NSCLC group but showed low abundance in the verification cohort. However, western blotting results indicated higher APOD expression in patients with NSCLC. These inconsistent results regarding APOD expression using different assays highlight the need for further investigations in larger cohorts. Similar to previous findings, western blotting results revealed upregulation of MVP, GYS1 and SERPINA3 in EVs from patients with NSCLC, suggesting that these biomarkers may promote lung cancer progression via EVs through mechanisms such as drug resistance, metabolic reprogramming, and apoptosis inhibition. However, the expression and function of HECTD3, SERPING1, TPM4 and APOD in lung cancer require further study.

Interestingly, regardless of immune enrichment, the biomarker panel could significantly distinguish between patients with can-

cer and healthy individuals. This indicates that the established biomarker panel reliably represents TDEVs and thus has the potential application for NSCLC liquid biopsy. Notably, CD155, a bait protein for enriching CD155+ TDEVs, was not included in the diagnostic panel because its expression density was below the PRM-targeted proteomics detection threshold. Considering the intricate heterogeneity of cancers, future research should integrate spatiotemporal omics and ultra-sensitive detection method to map the associations between tumour evolution and antigen fingerprints of TDEV, thus improving the reliability of liquid biopsy (Liu et al. 2024; Yang et al. 2024).

In conclusion, this study revealed DEP characteristics of circulating TDEVs through proteomics and machine learning. We identified a biomarker panel showing diagnostic potential for NSCLC liquid biopsy as well as for facilitating to understand the underlying mechanisms of NSCLC progression.

#### Author Contributions

Ye Yuan, Dian-Bing Wang and Xian-En Zhang conceptualized the study. Hai Jiang, Rui Xue and Lian Li collected the clinical samples. Xian-En Zhang, Dian-Bing Wang, Xiao-Jun Feng and Bi-Feng Liu supervised the study. Ye Yuan performed the experiments, analysed the data and wrote the original draft. Hai Jiang, Rui Xue, Bo Peng, Chen-Shuo Ren, Shi-Min Li and Min Li performed the statistical analysis and provided valuable suggestions. Na Li collected MS-based proteomic data. Xian-En Zhang and Dian-Bing Wang reviewed and edited the manuscript. All the authors have read and approved the final version of the manuscript.

#### Acknowledgements

We thank the National Natural Science Foundation of China (Grant No. 21890743, 32271489) and the National Key Research and Development Program of China (Grant No. 2022YFA1205804, 2022YFC2303501). We are grateful to Fu-Quan Yang and Ji-Feng Wang of Key Laboratory of Protein and Peptide Pharmaceuticals and Laboratory of Proteomics, IBP-CAS, for valuable technical supports in proteomics. Thanks to Jun-Ying Jia and Shu Meng of Institute of Biophysics, CAS, for the technical support in flow cytometry. Thanks to Li Wang and Long-Long Zhang of Centre for Biological Imaging (CBI), IBP-CAS, for their help of making EM samples and taking EM images. Thanks to Prof. Chang Chen for the gift of the pLVX-T2A-mCherry-Puro plasmid.

#### Conflicts of Interest

The authors declare no conflicts of interest.

#### Data Availability Statement

All data needed to evaluate the conclusions in the paper are present in the paper and/or the supplementary materials. The mass spectrometry proteomics data have been deposited into the ProteomeXchange Consortium via the iProX (Ma et al. 2019) partner repository with the dataset identifiers ProteomeXchange: PXD054691.

#### References

- Barlin, M., P. Erdmann-Gilmore, J. L. Mudd, et al. 2023. "Proteins in Tumor-Derived Plasma Extracellular Vesicles Indicate Tumor Origin." *Molecular & Cellular Proteomics* 22: 100476.
- Belov, L., K. J. Matic, S. Hallal, O. G. Best, S. P. Mulligan, and R. I. Christopherson. 2016. "Extensive Surface Protein Profiles of Extracellular Vesicles From Cancer Cells May Provide Diagnostic Signatures From Blood Samples." *Journal of Extracellular Vesicles* 5: 25355.

- Brlic, P. K., T. L. Rovis, G. Cinamon, P. Tsukerman, O. Mandelboim, and S. Jonjic. 2019. "Targeting PVR (CD155) and Its Receptors in Anti-Tumor Therapy." *Cellular & Molecular Immunology* 16: 40–52.
- Chen, W., Z. S. Xie, F. Q. Yang, and K. Q. Ye. 2017. "Stepwise Assembly of the Earliest Precursors of Large Ribosomal Subunits in Yeast." *Nucleic Acids Research* 45: 6837–6847.
- Chiang, E. Y., and I. Mellman. 2022. "TIGIT-CD226-PVR Axis: Advancing Immune Checkpoint Blockade for Cancer Immunotherapy." *Journal for Immunotherapy of Cancer* 10: e004711.
- Dixon, A. C., T. R. Dawson, D. di Vizio, and A. M. Weaver. 2023. "Context-Specific Regulation of Extracellular Vesicle Biogenesis and Cargo Selection." *Nature Reviews Molecular Cell Biology* 24: 454–476.
- Dong, Y., Q. H. Yuan, J. Ren, et al. 2023. "Identification and Characterization of a Novel Molecular Classification Incorporating Oxidative Stress and Metabolism-Related Genes for Stomach Adenocarcinoma in the Framework of Predictive, Preventive, and Personalized Medicine." *Frontiers in Endocrinology* 14: 1090906.
- Fitzgerald, R. C., A. C. Antoniou, L. Fruk, and N. Rosenfeld. 2022. "The Future of Early Cancer Detection." *Nature Medicine* 28: 666–677.
- Freed-Pastor, W. A., L. J. Lambert, and Z. A. Ely, et al. 2021. "The CD155/TIGIT Axis Promotes and Maintains Immune Evasion in Neoantigen-Expressing Pancreatic Cancer." *Cancer Cell* 39: 1342–1360e14.
- Giatromanolaki, A., E. Sivridis, S. Arelaki, and M. I. Koukourakis. 2017. "Expression of Enzymes Related to Glucose Metabolism in Non-Small Cell Lung Cancer and Prognosis." *Experimental Lung Research* 43: 167–174.
- Group F-NBW. 2016. *BEST (Biomarkers, EndpointS, and other Tools) Resource. 2016* (US FDA).
- Herbst, R. S., D. Morgensztern, and C. Boshoff. 2018. "The Biology and Management of Non-Small Cell Lung Cancer." *Nature* 553: 446–454.
- Hoshino, A., H. S. Kim, L. Bojmar, et al. 2020. "Extracellular Vesicle and Particle Biomarkers Define Multiple Human Cancers." *Cell* 182: 1044.
- Hu, T., J. Wolfram, and S. Srivastava. 2021. "Extracellular Vesicles in Cancer Detection: Hopes and Hypes." *Trends in Cancer* 7: 122–133.
- Huang, L., D. B. Wang, N. Singh, F. Yang, N. Gu, and X. E. Zhang. 2018. "A Dual-Signal Amplification Platform for Sensitive Fluorescence Biosensing of Leukemia-Derived Exosomes." *Nanoscale* 10: 20289–20295.
- Hulmi, J. J., F. Penna, N. Pöllänen, et al. 2020. "Muscle NAD Depletion and Serpina3n as Molecular Determinants of Murine Cancer Cachexia-The Effects of Blocking Myostatin and Activins." *Molecular Metabolism* 41: 101046.
- Jain, K. K., and K. K. Jain. 2010. *The Handbook of Biomarkers* (Springer).
- Jakobsen, K. R., B. S. Paulsen, R. Bæk, K. Varming, B. S. Sørensen, and M. M. Jørgensen. 2015. "Exosomal Proteins as Potential Diagnostic Markers in Advanced Non-Small Cell Lung Carcinoma." *Journal of Extracellular Vesicles* 4: 26659.
- Jeppesen, D. K., A. M. Fenix, J. L. Franklin, et al. 2019. "Reassessment of Exosome Composition." *Cell* 177: 428–+.
- Jin, A. L., C. Y. Zhang, W. J. Zheng, et al. 2022. "CD155/SRC Complex Promotes Hepatocellular Carcinoma Progression Via Inhibiting the p38 MAPK Signalling Pathway and Correlates With Poor Prognosis." *Clinical and Translational Medicine* 12: e794.
- Jin, X., Y. Chen, H. Chen, et al. 2017. "Evaluation of Tumor-Derived Exosomal miRNA as Potential Diagnostic Biomarkers for Early-Stage Non-Small Cell Lung Cancer Using Next-Generation Sequencing." *Clinical Cancer Research* 23: 5311–5319.
- Jin, Y., Y. Z. Peng, J. Xu, et al. 2024. "LUBAC Promotes Angiogenesis and Lung Tumorigenesis by Ubiquitinating and Antagonizing Autophagic Degradation of HIF1 $\alpha$ ." *Oncogenesis* 13: 6.
- Jung, Y. J., E. Katilius, R. M. Ostroff, et al. 2017. "Development of a Protein Biomarker Panel to Detect Non-Small-Cell Lung Cancer in Korea." *Clinical Lung Cancer* 18: E99–E107.
- Kalra, H., R. J. Simpson, H. Ji, et al. 2012. "Vesiclepedia: A Compendium for Extracellular Vesicles With Continuous Community Annotation." *PLOS Biology* 10: e1001450.
- Karsdal, M. A., K. Henriksen, D. J. Leeming, et al. 2009. "Biochemical Markers and the FDA Critical Path: How Biomarkers May Contribute to the Understanding of Pathophysiology and Provide Unique and Necessary Tools for Drug Development." *Biomarkers* 14: 181–202.
- Kawamura, K., Y. Komohara, K. Takaishi, H. Katabuchi, and M. Takeya. 2009. "Detection of M2 Macrophages and Colony-Stimulating Factor 1 Expression in Serous and Mucinous Ovarian Epithelial Tumors." *Pathology International* 59: 300–305.
- Krajewska, M., L. H. Smith, J. Rong, et al. 2009. "Image Analysis Algorithms for Immunohistochemical Assessment of Cell Death Events and Fibrosis in Tissue Sections." *Journal of Histochemistry and Cytochemistry* 57: 649–663.
- Lane, R. E., D. Korbie, M. M. Hill, and M. Trau. 2018. "Extracellular Vesicles as Circulating Cancer Biomarkers: Opportunities and Challenges." *Clinical and Translational Medicine* 7: 14.
- Lei, Y. M., X. C. Fei, Y. Ding, et al. 2023. "Simultaneous Subset Tracing and miRNA Profiling of Tumor-Derived Exosomes via Dual-Surface-Protein Orthogonal Barcoding." *Science Advances* 9: eadi1556.
- Li, M., X. H. Sun, J. Zhao, et al. 2020. "CCL5 Deficiency Promotes Liver Repair by Improving Inflammation Resolution and Liver Regeneration Through M2 Macrophage Polarization." *Cellular & Molecular Immunology* 17: 753–764.
- Li, N., B. W. Wu, and J. F. Wang, et al. 2023. "Differential Proteomic Patterns of Plasma Extracellular Vesicles Show Potential to Discriminate  $\beta$ -Thalassemia Subtypes." *iScience* 26: 106048.
- Li, Y., X. Chen, Z. H. Wang, et al. 2013. "The HECTD3 E3 Ubiquitin Ligase Suppresses Cisplatin-Induced Apoptosis via Stabilizing MALT1." *Neoplasia* 15: 39.
- Li, Y., Y. Kong, Z. Zhou, et al. 2013. "The HECTD3 E3 Ubiquitin Ligase Facilitates Cancer Cell Survival by Promoting K63-Linked Polyubiquitination of Caspase-8." *Cell Death & Disease* 4: e935.
- Li, Y., X. W. Wu, L. Li, et al. 2017. "The E3 Ligase HECTD3 Promotes Esophageal Squamous Cell Carcinoma (ESCC) Growth and Cell Survival Through Targeting and Inhibiting Caspase-9 Activation." *Cancer Letters* 404: 44–52.
- Liu, L., A. Chen, Y. Li, J. Mulder, H. Heyn, and X. Xu. 2024. "Spatiotemporal Omics for Biology and Medicine." *Cell* 187: 4488–4519.
- Liu, L., Y. Wang, C. Geng, et al. 2021. "CD155 Promotes the Progression of Cervical Cancer Cells Through AKT/mTOR and NF-kappaB Pathways." *Frontiers in Oncology* 11: 655302.
- Lou, L., J. Wang, F. Z. Lv, et al. 2021. "Y-Box Binding Protein 1 (YB-1) Promotes Gefitinib Resistance in Lung Adenocarcinoma Cells by Activating AKT Signaling and Epithelial-Mesenchymal Transition Through Targeting Major Vault Protein (MVP)." *Cellular Oncology* 44: 109–133.
- Lucien, F., D. Gustafson, M. Lenassi, et al. 2023. "MiBlood-EV: Minimal Information to Enhance the Quality and Reproducibility of Blood Extracellular Vesicle Research." *Journal of Extracellular Vesicles* 12: 12385.
- Luo, A. R., X. X. Lan, Q. Z. Qiu, et al. 2022. "LncRNA SFTA1P Promotes Cervical Cancer Progression by Interaction With PTBP1 to Facilitate TPM4 mRNA Degradation." *Cell Death & Disease* 13: 936.
- Ma, J., T. Chen, S. F. Wu, et al. 2019. "iProX: An Integrated Proteome Resource." *Nucleic Acids Research* 47: D1211–D1217.
- Marin, A. M., M. Batista, A. L. K. de Azevedo, et al. 2023. "Screening of Exosome-Derived Proteins and Their Potential as Biomarkers in Diagnostic and Prognostic for Pancreatic Cancer." *International Journal of Molecular Sciences* 24: 12604.
- Mathivanan, S., J. W. Lim, B. J. Tauro, H. Ji, R. L. Moritz, and R. J. Simpson. 2010. "Proteomics Analysis of A33 Immunoaffinity-Purified Exosomes Released From the Human Colon Tumor Cell Line LIM1215 Reveals a

- Tissue-Specific Protein Signature.” *Molecular & Cellular Proteomics* 9: 197–208.
- Mehana, M. R., S. A. Williams, J. M. Siegfried, et al. 2014. “Validation of a Blood Protein Signature for Non-Small Cell Lung Cancer.” *Clinical Proteomics* 11: 32.
- Miranda, E., F. Vizoso, A. Martín, et al. 2003. “Apolipoprotein D Expression in Cutaneous Malignant Melanoma.” *Journal of Surgical Oncology* 83: 99–105.
- Molina, J. R., P. G. Yang, S. D. Cassivi, S. E. Schild, and A. A. Adjei. 2008. “Non-Small Cell Lung Cancer: Epidemiology, Risk Factors, Treatment, and Survivorship.” *Mayo Clinic Proceedings* 83: 584–594.
- Ostenfeld, M. S., S. G. Jensen, D. K. Jeppesen, et al. 2016. “miRNA Profiling of Circulating EpCAM<sup>+</sup> Extracellular Vesicles: Promising Biomarkers of Colorectal Cancer.” *Journal of Extracellular Vesicles* 5: 31488.
- Pan, X. Y., J. Wang, L. J. Guo, et al. 2022. “Identifying a Confused Cell Identity for Esophageal Squamous Cell Carcinoma.” *Signal Transduction and Targeted Therapy* 7: 122.
- Poggio, M., T. Y. Hu, C. C. Pai, et al. 2019. “Suppression of Exosomal PD-L1 Induces Systemic Anti-Tumor Immunity and Memory.” *Cell* 177: 414.
- Qi, M. Y., Y. Xia, Y. J. Wu, et al. 2022. “Lin28B-High Breast Cancer Cells Promote Immune Suppression in the Lung Pre-Metastatic Niche via Exosomes and Support Cancer Progression.” *Nature Communications* 13: 897.
- Reck, M., and K. F. Rabe. 2017. “Precision Diagnosis and Treatment for Advanced Non-Small-Cell Lung Cancer.” *New England Journal of Medicine* 377: 849–861.
- Roumenina, L. T., M. V. Dagan, F. Petitprez, C. Sautès-Fridman, and W. H. Fridman. 2019. “Context-Dependent Roles of Complement in Cancer.” *Nature Reviews Cancer* 19: 698–715.
- Scheffer, G. L., A. B. Schroeijers, M. A. Izquierdo, E. A. C. Wiemer, and R. J. Scheper. 2000. “Lung Resistance-Related Protein/Major Vault Protein and Vaults in Multidrug-Resistant Cancer.” *Current Opinion in Oncology* 12: 550–556.
- Scheffer, G. L., P. L. J. Wijngaard, M. J. Flens, et al. 1995. “The Drug Resistance-Related Protein Lrp Is the Human Major Vault Protein.” *Nature Medicine* 1: 578–582.
- Siegel, R. L., A. N. Giaquinto, and A. Jemal. 2024. “Cancer Statistics, 2024.” *CA: A Cancer Journal for Clinicians* 74: 12–49.
- Stanley, P. 2011. “Golgi Glycosylation.” *Cold Spring Harbor Perspectives in Biology* 3: a005199.
- Sun, K. X., B. F. Han, H. M. Zeng, et al. 2024. “Incidence and Mortality of Cancers in Female Genital Organs—China, 2022.” *China CDC Weekly* 6, no. 10: 195–202.
- Tan, A. C., S. H. Tan, S. Q. Zhou, S. Peters, G. Curigliano, and D. S. W. Tan. 2022. “Efficacy of Targeted Therapies for Oncogene-Driven Lung Cancer in Early Single-Arm Versus Late Phase Randomized Clinical Trials: A Comparative Analysis.” *Cancer Treatment Reviews* 104: 102354.
- Tauro, B. J., D. W. Greening, R. A. Mathias, S. Mathivanan, H. Ji, and R. J. Simpson. 2013. “Two Distinct Populations of Exosomes Are Released From LIM1863 Colon Carcinoma Cell-Derived Organoids.” *Molecular & Cellular Proteomics* 12: 587–598.
- Thuya, W. L., L. R. Kong, N. L. Syn, et al. 2023. “FAM3C in Circulating Tumor-derived Extracellular Vesicles Promotes Non-small Cell Lung Cancer Growth in Secondary Sites.” *Theranostics* 13: 621–638.
- Tsolou, A., D. Koparanis, I. Lamprou, A. Giatromanolaki, and M. Koukourakis. 2023. “Increased Glucose Influx and Glycogenesis in Lung Cancer Cells Surviving After Irradiation.” *International Journal of Radiation Biology* 99: 692–701.
- van Niel, G., G. D’Angelo, and G. Raposo. 2018. “Shedding Light on the Cell Biology of Extracellular Vesicles.” *Nature Reviews Molecular Cell Biology* 19: 213–228.
- Wang, D. J., Y. M. Gu, X. Yan, et al. 2022. “Role of CD155/TIGIT in Digestive Cancers: Promising Cancer Target for Immunotherapy.” *Frontiers in Oncology* 12: 844260.
- Wang, Y. M., C. L. Li, Z. M. Wang, et al. 2022. “Comparison Between Immunotherapy Efficacy in Early Non-Small Cell Lung Cancer and Advanced Non-Small Cell Lung Cancer: A Systematic Review.” *BMC Medicine* 20: 426.
- Wang, Z., H. Chen, L. Sun, et al. 2024. “Uncovering the Potential of APOD as a Biomarker in Gastric Cancer: A Retrospective and Multi-Center Study.” *Computational and Structural Biotechnology Journal* 23: 1051–1064.
- Williams, P. A., S. K. Zaidi, and R. Sengupta. 2023. “AACR Cancer Progress Report 2023: Advancing the Frontiers of Cancer Science and Medicine.” *Clinical Cancer Research* 29: 3850–3851.
- Xing, Z. S., S. L. Li, Z. X. Liu, C. Zhang, and Z. M. Bai. 2021. “CircSERPINA3 Regulates SERPINA3-Mediated Apoptosis, Autophagy and Aerobic Glycolysis of Prostate Cancer Cells by Competitively Binding to MiR-653-5p and Recruiting BUD13.” *Journal of Translational Medicine* 19: 492.
- Xu, R., A. Rai, M. S. Chen, W. Suwakulsiri, D. W. Greening, and R. J. Simpson. 2018. “Extracellular Vesicles in Cancer—implications for Future Improvements in Cancer Care.” *Nature Reviews Clinical Oncology* 15: 617–638.
- Yang, C. Y., J. W. Sun, Y. L. Zhang, et al. 2024. “Construction of AlGaIn/GaN High-Electron-Mobility Transistor-Based Biosensor for Ultrasensitive Detection of SARS-CoV-2 Spike Proteins and Virions.” *Biosensors & Bioelectronics* 257: 116171.
- Yang, R., G. Zheng, D. F. Ren, et al. 2018. “The Clinical Significance and Biological Function of Tropomyosin 4 in Colon Cancer.” *Biomedicine & Pharmacotherapy* 101: 1–7.
- Yuan, Q., S. Q. Wang, G. T. Zhang, et al. 2021. “Highly Expressed of SERPINA3 Indicated Poor Prognosis and Involved in Immune Suppression in Glioma.” *Immunity, Inflammation and Disease* 9: 1618–1630.
- Zhan, M. X., Z. R. Zhang, X. G. Zhao, et al. 2022. “CD155 in Tumor Progression and Targeted Therapy.” *Cancer Letters* 545: 215830.
- Zhang, G. H., Q. Z. Zhu, X. M. Yan, et al. 2022. “HECTD3 Promotes Gastric Cancer Progression by Mediating the Polyubiquitination of c-MYC.” *Cell Death Discovery* 8: 185.
- Zhang, Q., R. Abdo, C. Iosef, et al. 2022. “The Spatial Transcriptomic Landscape of Non-Small Cell Lung Cancer Brain Metastasis.” *Nature Communications* 13: 5983.
- Zhang, Q., E. Z. Wu, Y. H. Tang, et al. 2021. “Deeply Mining a Universe of Peptides Encoded by Long Noncoding RNAs.” *Molecular & Cellular Proteomics* 20: 100109.
- Zhang, Y. P., J. Y. Sun, M. Li, et al. 2024. “Identification and Validation of a Disulfidptosis-Related Genes Prognostic Signature in Lung Adenocarcinoma.” *Heliyon* 10: e23502.
- Zhao, X. T., M. Jiang, and Z. Y. Wang. 2019. “TPM4 Promotes Cell Migration by Modulating F-Actin Formation in Lung Cancer.” *Oncotargets and Therapy* 12: 4055–4063.
- Zhou, R. J., S. Y. Chen, Q. W. Wu, et al. 2023. “CD155 and Its Receptors in Cancer Immune Escape and Immunotherapy.” *Cancer Letters* 573: 216381.
- Zhou, X. W., Y. Li, X. R. Zhang, et al. 2024. “Hemin Blocks TIGIT/PVR Interaction and Induces Ferroptosis to Elicit Synergistic Effects of Cancer Immunotherapy.” *Science China-Life Sciences* 67: 611–613.
- Zibert, A., and E. Wimmer. 1992. “N-Glycosylation of the Virus Binding Domain is Not Essential for Function of the Human Poliovirus Receptor.” *Journal of Virology* 66: 7368–7373.

## Supporting Information

Additional supporting information can be found online in the Supporting Information section.